An investigation into the local segmental dynamics of polyethylene: An isothermal/isobaric molecular dynamics study

S. D. Hotston, D. B. Adolf,[a] and K. Karatasos
Department of Physics and Astronomy, University of Leeds, Leeds LS2 9JT, United Kingdom

Molecular dynamics simulations of unentangled linear polyethylene melts have been performed for systems composed of 10 chains of 100 united atoms over a pressure range of 1 to 5000 bar and a temperature range of 375 to 475 K. Transition rates, activation volumes, and activation energies are in good agreement with values from similar simulations quoted in literature for systems well above T_g. Second-neighbor torsional angle coupling is observed to increase with increasing pressure and decreasing temperature. The lifetime of this coupling between conformational events is presented for the first time. Geometric autocorrelation functions are analyzed in terms of their distribution of relaxation times and reveal a process on the time scale of a few picoseconds and another on the time scale of a few nanoseconds. An intermediate process develops between these two time scales at high pressure and low temperature. © *2001 American Institute of Physics.* [DOI: 10.1063/1.1381057]

I. INTRODUCTION

There is significant interest within the polymer community to clarify the structure-property relationships between bulk polymers and the chemical composition of their repeat unit. This connection has been addressed in terms of local motion occurring on the length scale of a few monomers. These motions are heavily influenced by the chemistry of the repeat unit and are also expected to be related to longer length scale motions responsible for the observed viscoelastic properties of polymers. Aspects of local dynamics appear in several fundamental theories and key experimental observations describing macromolecular rheology[1] and have been experimentally monitored by dielectric relaxation,[2,3] NMR,[4–6] and time-resolved optical spectroscopy.[7–14]

These motions have been studied within dilute polymer solutions as a function of solvent viscosity using thermodynamically good solvents where the dynamics are observed to scale by a fractional power of solvent viscosity, η.[5,14] This violates a hydrodynamic scaling prediction that the dynamics would scale by η to the first power and is attributed to the overlap of the time scales for local polymer dynamics and solvent reorientation. Within the melt, short length scale polymer dynamics become an essential mode of relaxation since chain congestion and chain entanglement create an enormous frictional resistance to large-scale reorientational motion of the polymer backbone. Several studies have revealed that the segmental dynamics of bulk polymers,[8,15–19] exhibits a temperature dependence as described by their William–Landel–Ferry [WLF] parameters associated with viscoelastic relaxation. These findings support the hypothesis that segmental dynamics is a valuable stepping stone in understanding the links between microscopic polymer structure and macroscopic polymer properties.

Additional insight has been provided through the use of computer simulation. Helfand and co-workers[20–22] used Brownian dynamics simulations to study the solution state dynamics of polyethylene which included a cataloguing of the conformation of chain torsional angles and the discovery of second-neighbor torsional angle coupling. The activation energy of the conformational transition rates was observed to be slightly larger than a single *trans* to *gauche* barrier height energy of the torsional angle potential employed. This implied that these processes cannot be pictured as crankshaft motions[23] which would require an activation energy of two barrier heights. Helfand labeled these motions cranklike. Adolf and Ediger[24] simulated the local motions of solution state polyisoprene and revealed a decrease in the amount of second-neighbor torsional angle coupling and an increase in the first-neighbor torsional angle coupling relative to Helfand's polyethylene findings. Moe and Ediger[25] simulated isolated and bulk polyisoprene using NVT molecular dynamics. Findings revealed that C–H vectors relax predominately by coupled small amplitude motions of groups of adjacent torsions which do not involve conformational transitions. NpT simulations of polyethylene due to Smith *et al.*[26,27] showed that correlation times for the torsional autocorrelation function and C–H vector reorientation correspond to the average conformational transition times. They also reveal significant second- and fourth-neighbor torsional angle coupling. Moro[28–30] has highlighted the importance of small displacements of torsional angles within the conformational dynamics of chained molecules. This work also suggested that the time taken for neighbors to feel a conformational event increases with the distance from the torsional angle undergoing the event.

Fewer studies of segmental polymer dynamics have focused on the impact of pressure, which is surprising due to its importance in polymer processing and applications. Williams[19,31] used dielectric spectroscopy to probe the dynamics of poly(methylacrylate) at high pressure. The observed relaxation times were found to be a function of two

---

[a] Author to whom correspondence should be addressed. Electronic mail: d.b.adolf@leeds.ac.uk

2359   © 2001 American Institute of Physics

components. One is dependent on both pressure and temperature, with the other dependent only on temperature. Sasabe and Saito[32] observed for poly(alkylmethacrylates) that the segmental motions of the backbone (denoted as the α process) and side chain motions (denoted as the β process) are decoupled at low temperature or high pressure. However, these motions couple as temperature is increased or pressure is decreased affording a single $\alpha\beta$ dynamic. In the late 1980s to early 1990s, the pressure-induced slowing of local segmental polymer dynamics was monitored using the pressure dependence of the fluorescence lifetime of an intramolecular excimer-forming probe dispersed within a matrix of polyisoprene, polyisobutylene, or poly(propylene oxide).[33–35] Efforts due to Kulik and Prins[36–39] employed NMR to study bulk polystyrene dynamics under pressures of up to 2500 bar. They reported a gradual increase in the mean correlation time and distribution width for conformational dynamics with increasing pressure. Floudas and co-workers[40–42] used dielectric relaxation to investigate the effect of high pressure on the segmental and normal mode dynamics of polyisoprene and polyisoprene/polyvinylethylene diblock copolymers. Findings for the diblock samples reveal that pressure induces dynamic homogeneity. Furthermore, the segmental dynamics of polyisoprene was observed to be more sensitive to pressure than the corresponding normal mode dynamics, implying failure of time-pressure superposition. Computationally, Bharadwaj and Boyd[43] have examined the effects of temperature and pressure on the local dynamics, showing that increasing pressure and reducing temperature lead to spatial heterogeneity of conformational transitions along the backbone.

The current work reports on a computational study to understand the effect of systematic changes in pressure on local segmental dynamics, similar in spirit to the work of Karatasos *et al.*[44] on the role of systematic increases of density on these motions. NpT simulations of linear unentangled polyethylene melts have been performed up to pressures of 5000 bar. Polyethylene is chosen for its technological importance and structural simplicity. The procedure for the construction of the initial configurations and other algorithmic details are found in Sec. II. Section III verifies the integrity of the equilibrated melt configurations through activation energies, activation volumes, and equation of state behavior. Section IV addresses the effect of pressure on torsional angle coupling. This analysis is presented as a function of distance along the backbone at a fixed time and also as a function of backbone distance and time after a conformational triggering event. An examination of the effects of pressure on the local segmental dynamics is presented through geometric autocorrelation functions and associated distributions of relaxation times (DRT) as found within Sec. V. Conclusions are found within Sec. VI.

II. SIMULATION DETAIL

A. Initialization and algorithm particulars

The starting configurations were generated by a lattice Monte Carlo procedure via the cooperative motion algorithm (CMA).[45,46] This algorithm is capable of operating at high densities, affording equilibrated melt configurations at a low computational cost. After placing several thousand chains, each composed of 100 united atoms, on a face-centered cubic (fcc) lattice, the initial arrangement was ''melted'' through cooperative rearrangements in the athermal limit, where all the attempted moves which avoided monomer–monomer overlaps and which preserved the chain connectivity were accepted. After complete relaxation at a local and a global length scale as probed by the bond and the end-to-end vector autocorrelation functions,[44] a subset of chains was randomly selected among those with a density close to the targeted one. Following the introduction of valence angles and bond constraints as given in Sec. II B, the system was fine tuned to the target density by translating the chains toward the subset's center of mass in small steps to avoid overlaps. At this stage, the target density of these configurations was 0.79 g/cm^3 corresponding to the accepted value of bulk polyethylene at a pressure of 1 bar and a temperature of 400 K.[47]

The trajectories are generated in two stages. The starting configurations provided by the sampling technique are further equilibrated at 400 K for 6 ns using the Nosé–Hoover NVT algorithm[48,49] with a thermostat relaxation coefficient of 0.1 ps. This is followed by 10 ns of equilibration using an NpT ensemble at the eventual production temperature and pressure, the thermostat and barostat relaxation coefficients being 0.1 and 0.21 ps, respectively.[50] Following equilibration, 10 ns of production is performed at 1, 1000, and 5000 bar, each generated at 375, 400, 425, 450, and 475 K.

B. Simulation parameters

The application used to generate the trajectories discussed in this paper is the DL_POLY (V2.10) Molecular Dynamics package.[51] A Verlet leapfrog scheme with a time step of 2 femtoseconds is used to integrate the equation of motion and the SHAKE algorithm is used to maintain bond lengths of 1.53 Å.

The valence angle potential is of the form

$$V(\theta) = \tfrac{1}{2}k_\theta(\cos\theta - \cos\theta_0)^2, \tag{1}$$

where $k_\theta = 519.6$ kJ/mol and $\theta_0 = 112.813°$.

The torsional angle potential is based on the widely used[26,27,52,53] version derived by Jorgensen and Tirado-Rives[54] and has the form

$$\frac{V(\phi)}{\text{kJ/mol}} = 2.937(1 + \cos(\phi)) + 0.565(1 - \cos(2\phi))$$

$$+ 6.544(1 + \cos(3\phi)), \tag{2}$$

with prefactors being taken from the work of Martin and Siepmann[55] on n-alkanes at the critical temperature.

The nonbonded interactions are based on an optimized Lennard-Jones potential for n-alkanes,[55] where two atoms i and j, being separated by a distance of r_{ij} as shown in Eq. (3), are modeled with distinct values of ε and σ for the CH_3 and CH_2 units, as shown in Table 1:

$$V(r_{ij}) = 4\varepsilon\left[\left(\frac{\sigma}{r_{ij}}\right)^{12} - \left(\frac{\sigma}{r_{ij}}\right)^6\right]. \tag{3}$$

TABLE I. Lennard-Jones parameters (Ref. 55).

	σ (Å)	ε (kJ/mol)
CH_2-CH_2	3.95	0.381
CH_3-CH_3	3.75	0.808
CH_2-CH_3	3.85	0.556

III. CONFORMATIONAL ACTIVITY AND THERMODYNAMICS

A. Transition rate

The definition of what constitutes a conformational transition has appeared in many studies with slightly different definitions.[23,43,44,56–58] A definition similar to that used by Helfand[21,22,44,59–62] is employed throughout this work. A stopwatch is started when a torsional angle first leaves a window of 40° in width which is centered on one of the three minima (i.e., *trans*, *gauche* plus, and *gauche* minus) defined by Eq. (2). This window is chosen to focus on conformational activity rather than libration. The stopwatch is stopped when the torsional angle first passes the minimum of a neighboring well.

The effects of the more mobile chain ends have been removed by excluding the transition rates of the ten outer torsional angles of each molecule from the appropriate analyses. In Table II, the average transition rate is shown together with comparisons to literature values. For 400 K at 1 and 5000 bar, average transition rates are 0.059 and 0.041 ps^{-1}, respectively. Bharadwaj and Boyd report comparable average transition rates of 0.060 and 0.043 ps^{-1} for a united atom system of 768 CH_2 beads at 400 K with pressures of 1 and 5000 bar, respectively.[43] For an explicit atom melt of $C_{44}H_{90}$ chains at 400 K and 1 bar, Smith *et al.* observed a similar average transition rate of 0.060 ps^{-1}.[52]

B. Activation volume and activation energy

The activation volume is calculated as

$$\Delta V = RT \left(\frac{\partial \ln \tau_0}{\partial p} \right)_T, \tag{4}$$

where

$$\tau_0 \sim \exp(\Delta G / RT). \tag{5}$$

TABLE II. Transition rate (ps^{-1}) for all systems (± 0.001 for all values reported from this study).

Temperature (K)	1 bar	1000 bar	5000 bar
375	0.043	0.040	0.029
400	0.059	0.051	0.041
400[a]	0.060	⋯	0.043
400[b]	0.060	⋯	⋯
425	0.069	0.062	0.052
450	0.085	0.074	0.065
475	0.097	0.090	0.078

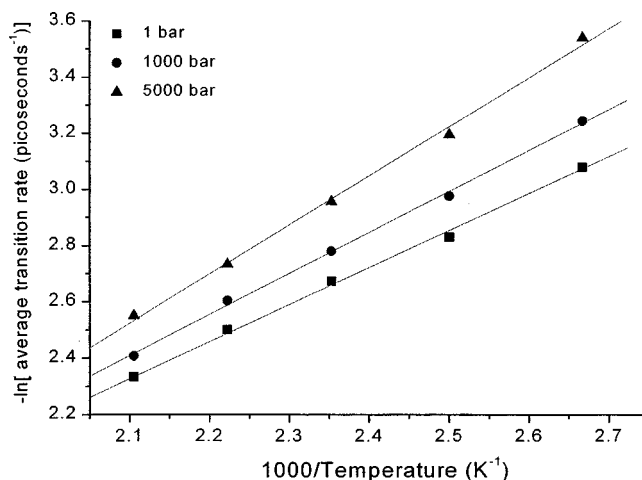[a]Reference 43.
[b]Reference 52.

FIG. 1. The negative natural logarithm of the average transition rate per picosecond at 1, 1000, and 5000 bar as a function of temperature. Best-fit lines are illustrated for each pressure. The slope of each best-fit line is used to determine the activation enthalpy.

τ_0 is the average time between conformational transitions for the system and ΔG is the Gibbs free energy

$$\Delta G = \Delta E + p\Delta V - T\Delta S. \tag{6}$$

ΔE, ΔV, and ΔS are the energy, volume, and entropy of activation, respectively. As the motion per transition is small, the change in entropy is considered to be negligible.[39]

The activation enthalpy is defined as

$$\Delta H = \Delta E + p\Delta V, \tag{7}$$

and is calculated as

$$\Delta H = R \left(\frac{\partial \ln \tau_0}{\partial (1000/T)} \right)_p. \tag{8}$$

The negative natural logarithm of the average transition rate per dihedral per picosecond is plotted against inverse temperature in Fig. 1 at different pressures with data at each pressure connected by a line of best fit. The data show that the natural logarithm of the average transition time changes
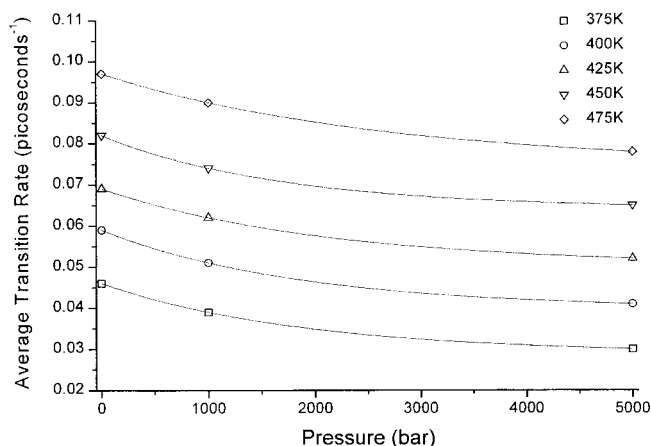

FIG. 2. The average transition rate per picosecond over a temperature range of 375 to 475 K as a function of pressure. Best-fit single exponential curves are illustrated for each set of data points.
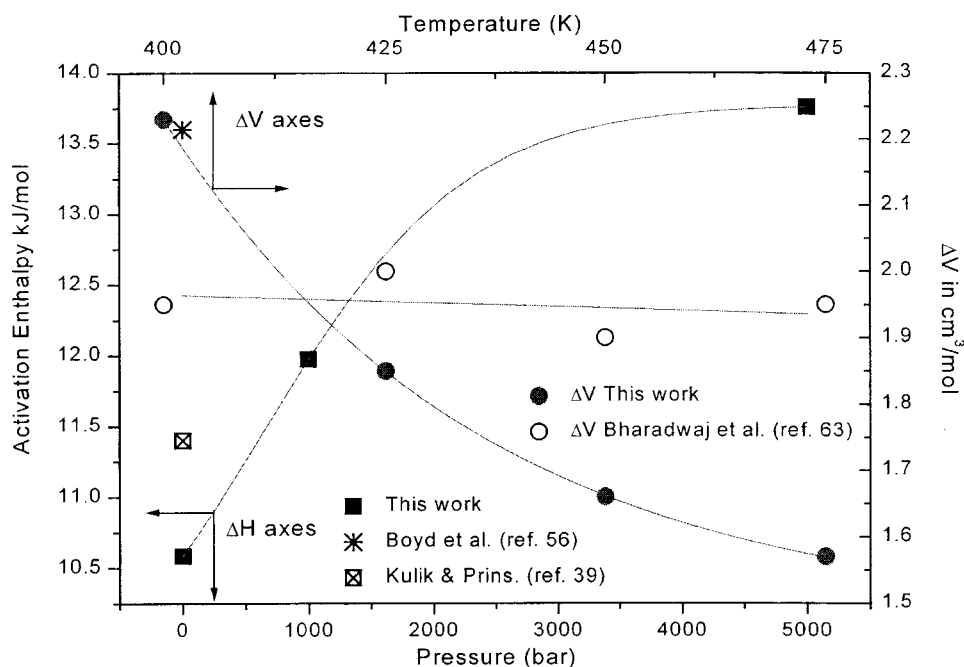
FIG. 3. The pressure dependence of the activation enthalpy (filled squares) is observed using the left and bottom axes. The temperature dependence of the activation volume (filled circles) is observed using the right and top axes. Comparison is made with results from Boyd et al. (Ref. 56) and Kulik and Prins (Ref. 39) for the activation enthalpy and Bharadwaj et al. (Ref. 63) for the activation volume. Lines are a guide to the eye and errors are contained within symbol size.

linearly with inverse temperature for pressures of 1, 1000, and 5000 bar. Figure 2 shows the average transition rate per torsional angle per picosecond decreases with increasing pressure for each pressure studied as illustrated by the single exponential best-fit curves. An average dT/dp value of 0.017 $\pm$0.002 deg/bar is obtained from Figs. 1 and 2 for the pressure range of 1 to 1000 bar over the five simulated temperatures. This is in good agreement with literature.[39,42,43] dT/dp serves as a gauge for the inter-relation effects of temperature and pressure on relaxation times and for many polymers its magnitude is approximately 0.020$\pm$0.005 deg/bar.[1] Kulik and Prins used deuteron NMR to study amorphous polyethylene between 203 and 393 K and up to 2500 bar to obtain a value of 0.015 deg/bar. In a study of the dielectric relaxation of polyisoprene at pressures of up to 5000 bar, Floudas et al. report a comparable figure of 0.016 deg/bar. If the data within Figs. 1 and 2 at 5000 bar are considered at each simulated temperature, dT/dp is found to be 0.010$\pm$0.002 deg/bar. Bharadwaj and Boyd report a dT/dp of 0.01 deg/bar from a simulation of polyethylene up to 10 000 bar.

The activation volumes for torsional angle rotation in Å^3 per torsional angle at different temperatures are computed using Eq. (4) and shown in Fig. 3. Table III reports the activation volume in cubic centimeters per mole as a function of temperature. Activation volumes from Bharadwaj and

Boyd[63] are also plotted in Fig. 3 and are included within Table III. These values are qualitatively similar but less sensitive to temperature in comparison to the values reported in this manuscript. It is difficult to pinpoint the exact cause of this behavior but it might be attributed to the use of the anisotropic united atom model by Bharadwaj and Boyd.

Figure 3 also shows the activation energies at constant pressure, ranging from 1 to 5000 bar. The activation enthalpies are 10.6$\pm$0.1 kJ/mol (1 bar), 11.9$\pm$0.1 kJ/mol (1000 bar) and 13.7$\pm$0.1 kJ/mol (5000 bar). Comparisons are made with the work of Boyd et al.[56] and Kulik and Prins.[39] Boyd et al. report an activation enthalpy of 13.6 kJ/mol for a melt of polyethylene at 1 bar within the NpT ensemble for a 768 UA bead chain. Kulik and Prins calculated an experimental conformational transition activation enthalpy of 11.4 kJ/mol

TABLE III. Activation energies and volumes.

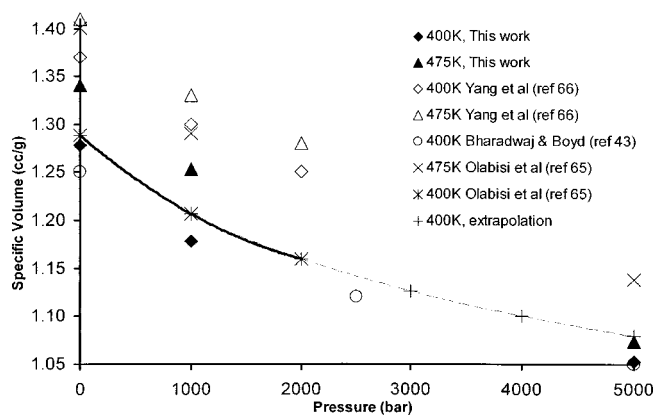|	1 bar	1000 bar	5000 bar	
ΔH (kJ/mol)	10.6$\pm$0.1	11.9$\pm$0.1	13.7$\pm$0.1	
	400 K	425 K	450 K	475 K
ΔV (cm^3/mol) (This work)	2.22	1.85	1.66	1.61
ΔV (cm^3/mol) (Bharadwaj and Boyd[a])	1.95	2.00	1.90	1.95

[a]Reference 63.

FIG. 4. The dependence of specific volume on pressure at constant temperature. The filled symbols represent data from this work while the crosses and the asterisks are experimental values from Olabisi and Simha and fit to the Tait equation (Ref. 65). The Tait equation is valid up to 2000 bar (solid line), with values extrapolated to 5000 bar denoted by plus signs connected by a dashed line. The open symbols are simulated values cited in literature from Yang et al. (Ref. 66) and Bharadwaj and Boyd (Ref. 43).

J. Chem. Phys., Vol. 115, No. 5, 1 August 2001

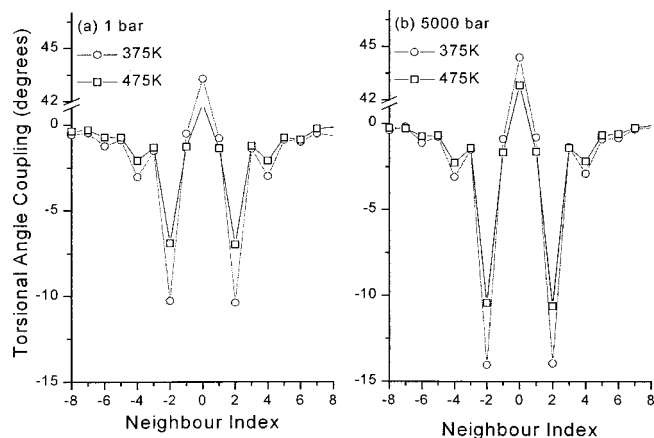Local segmental dynamics of polyethylene   2363

FIG. 5. Torsional angle coupling shown for 1 and 5000 bar at 375 and 475 K illustrating counter-rotational second-neighbor torsional angle coupling. Error is contained within the symbol size and lines are an aid to the eye.

at 1 bar. Both these values are in reasonable agreement with results reported here.[39,43,56,57,64] The magnitude of the $p\Delta V$ term is effectively zero at low pressures. At 5000 bar, it comprises nearly 10% of the overall activation enthalpy, with the maximum contribution to the activation enthalpy from the $p\Delta V$ term being about 1 kJ/mol. Kulik and Prins report 1.5 kJ/mol for the maximum contribution of the $p\Delta V$ term to ΔH.

C. Specific volume as a function of pressure and temperature

The specific volume as a function of temperature and pressure for the simulated systems has been calculated for all systems and the data for the 400 and 475 K systems are shown in Fig. 4 as filled symbols. This plot also contains the experimental specific volume as reported by Olabisi and Simha and fit to the Tait equation.[65] These data are shown as crosses and asterisks. At 400 K, the experimental data is valid up to 2000 bar and has been extrapolated to 5000 bar for the basis of a qualitative comparison and is plotted as plus signs. Computational data from Yang et al.[66] are plotted as hollow diamonds and triangles, with data from Bharadwaj
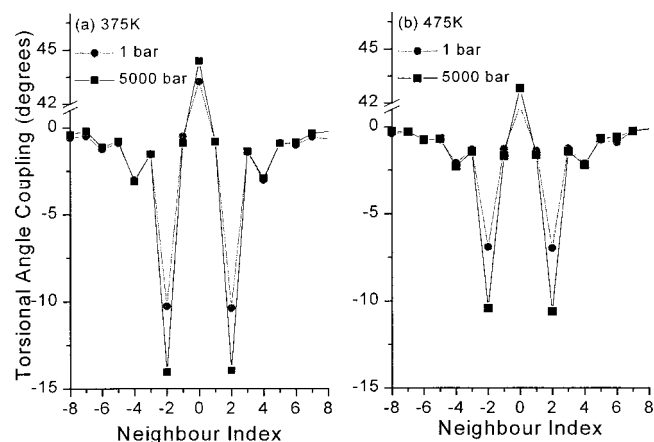

FIG. 6. Torsional angle coupling shown for 375 and 475 K at 1 and 5000 bar illustrating counter-rotational second-neighbor torsional angle coupling. Error is contained within the symbol size and lines are an aid to the eye.

TABLE IV. Absolute magnitude in degrees of second-neighbor torsional angle coupling for all systems.

	375 K	400 K	425 K	450 K	475 K
1 bar	10.5	10.0	9.5	8.5	7.0
1000 bar	12.5	11.5	10.5	9.0	8.5
5000 bar	14.5	13.5	12.5	11.5	10.5

and Boyd[43] denoted as open circles. The quality of agreement between the filled symbols and the Tait equation is good. However, the agreement is not surprising given that the simulation parameters of Martin and Siepmann are optimized for n-alkanes.

D. Pressure and the glass transition temperature

The computer glass transition temperature for this system at a pressure of 1 bar is expected to be in the vicinity of 200–250 K, based on results from similar simulations.[66,67] At 5000 bar, the computer glass transition temperature is expected to occur between 250 and 335 K using 0.010 deg/bar$\leqslant dT/dp \leqslant$0.017 deg/bar as reported in Sec. III B. The specific volume at 5000 bar was plotted over a temperature range of 300 to 475 K. These plots are not shown but they revealed that a single line successfully fit the data. The lack of a break in this slope in conjunction with the data presented in Figs. 1 through 4 suggests that suitably equilibrated nonglassy melts are being employed.

IV. ANALYSIS AND RESULTS

A. Static torsional angle coupling

Localization is an important factor in conformational motion, enabling torsional angles to rotate without invoking huge energy penalties associated with moving large sections of the backbone through a melt or viscous solvent. Localization can be understood through two mechanisms, coupled conformational motion[25,46,68,69] and coupled libration.[28–30,70–74] Following on from the work presented by Karatasos et al.,[44] the present trajectories have been analyzed with respect to torsional angle coupling via a method developed by Moe and Ediger.[25]

Torsional angle coupling, TAC(ϕ_i, τ_{TT}), is defined as the average change of a neighboring torsional angle, ϕ_i, in response to a triggering transition, TT, at time τ_{TT}. This is expressed as

$$\text{TAC}(\phi_i, \tau_{TT}) = \langle A(\Delta\phi_i) | \phi_i(\tau_{TT} + \Delta t) - \phi_i(\tau_{TT} - \Delta t)| \rangle, \tag{9}$$

where $A(\Delta\phi_i)$ assumes a value of $+1$ for ϕ_i motion in the same direction as the TT and -1 for ϕ_i motion in the opposite direction of the TT. The angular brackets denote an average over all torsional angles and over the entire production phase of the trajectory. Within this manuscript, the use of a single value for Δt in Eq. (9) is referred to as static torsional angle coupling analysis. Dynamic torsional angle coupling analysis is discussed in the following section, where a range of Δt values is employed.
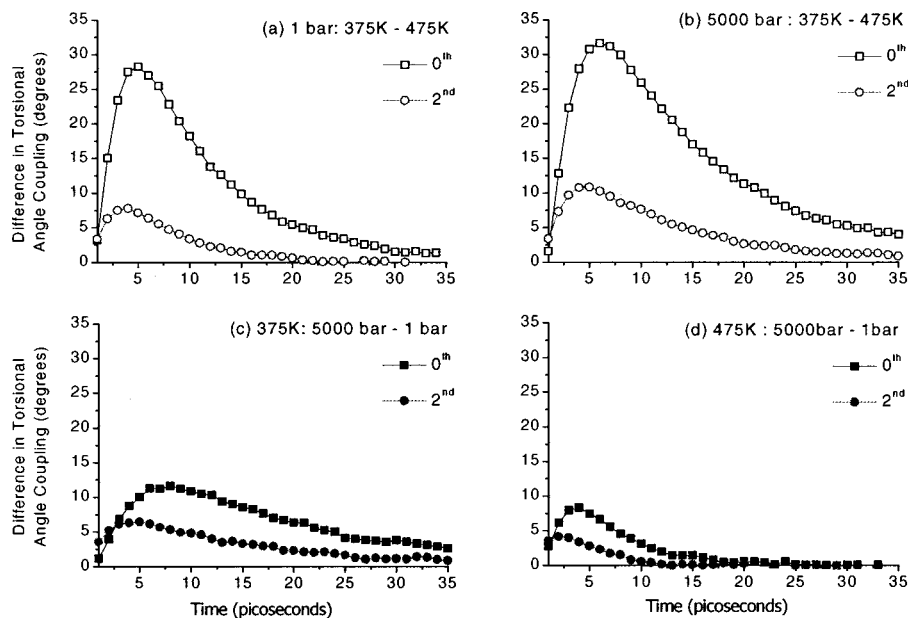
Figure 5 compares the magnitude of 375 and 475 K tor-

FIG. 7. Differences in the magnitude in torsional angle coupling are shown for (a) 375 K relative to 475 K at 1 bar. (b) 375 K relative to 475 K at 5000 bar. (c) 5000 bar relative to 1 bar at 375 K and (d) 5000 bar relative to 1 bar at 475 K. Absolute values of differences in the torsional angle coupling for the second neighbors are plotted for clarity. Consequently, the plotted differences reflect increases in their counter-rotational motion. Error is contained in the symbol and lines are an aid to the eye.

sional angle coupling at 1 and 5000 bar with a Δt of 1 ps. Error is contained within the symbol size and the lines joining data points are only an aid to the eye. As temperature is decreased, there is an increase in the magnitude of the zeroth and second neighbor torsional angle coupling at both pressures. Zeroth neighbor torsional angle coupling refers to $i = 0$ within Eq. (9), where motion of the torsional angle undergoing the triggering transition is being monitored within the time window Δt. At 1 bar, decreasing the temperature by 100 K increases the magnitude of second-neighbor torsional angle coupling from -7 to -10.5 ($\sim 50\%$), and at 5000 bar from -10.5 to -14.5 ($\sim 38\%$). The increase in the magnitude of the zeroth neighbor torsional angle coupling is 3 (less than 8%). The magnitude of fourth-neighbor torsional angle coupling increases from 2 to 3 (by 50%). Figure 6 compares the magnitude of the 1 and 5000 bar torsional angle coupling at 375 and 475 K. At 375 K, the increase in the magnitude of torsional angle coupling with pressure is from -10.5 to -14.5 for the second neighbor ($\sim 38\%$). At 475 K, the increase in the magnitude of second-neighbor torsional angle coupling is from -7 to -10.5 ($\sim 50\%$). For both systems, the increase in the magnitude of zeroth-neighbor torsional angle coupling is only about 1 ($<5\%$), with no change at all in the magnitude of the fourth-neighbor torsional angle coupling.

Table IV shows the absolute magnitude of torsional angle coupling for the second neighbors for all systems. The importance of these changes is emphasized when it is remembered that the average transition rate drops with decreasing temperature. For instance, cooling the 475 K, 1 bar system by 100 K results in an increase in the magnitude of the second-neighbor torsional angle coupling of $\sim 50\%$, while the transition rate decreases by $\sim 56\%$.

For both Figs. 5 and 6 it should be noted that the second neighbors always move in a predominantly counter-TT manner. The increase in the magnitude of the torsional angle coupling at high pressure and low temperature was addressed through histograms of the values that make up the plotted

average data [see Eq. (9)]. These plots are not shown but revealed that increases arise from changes over the entire distribution of torsional angles being accessed rather than from a select range of torsional angles.

B. Dynamic torsional angle coupling

It is possible to examine how long-lived torsional angle coupling is by varying the value of Δt in Eq. (9). This analysis provides both a qualitative and a quantitative measure of the dynamic behavior of torsional angle coupling. The zeroth- and second-neighbor torsional angle coupling has been calculated over a range of $\Delta t = 1$ to 50 ps averaged over all chains and all transitions and illustrated in Fig. 7. The data are presented so that the values plotted represent the increase in magnitude of zeroth- and second-neighbor tor-
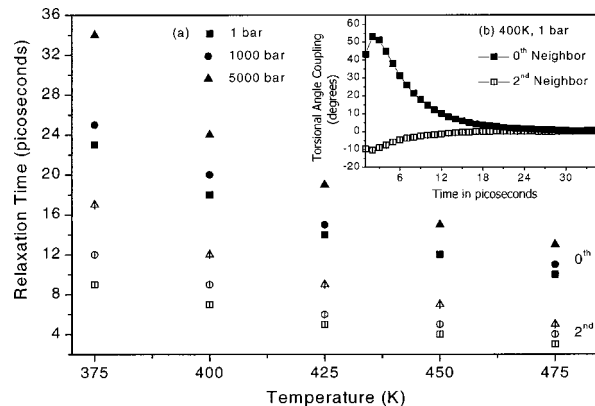

FIG. 8. The pressure and temperature dependence of the relaxation time for torsional angle coupling of zeroth neighbors (filled symbols) and second neighbors (open symbols). A relaxation time is defined as the time needed for the magnitude of the torsional angle coupling to decay to a background level of ± 2 as shown in panel (b) at 400 K and 1 bar.

TABLE V. Zeroth- and second-neighbor torsional angle coupling relaxation time for all systems in picoseconds.

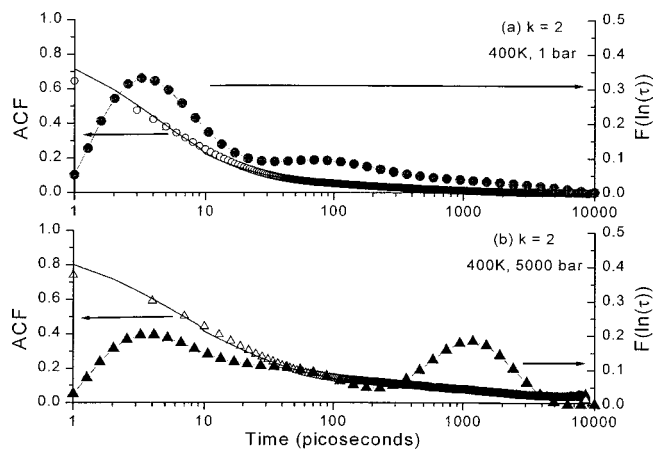|	375 K	400 K	425 K	450 K	475 K
Zeroth neighbor					
1 bar	23	18	14	12	10
1000 bar	25	20	15	13	11
5000 bar	34	24	19	15	13
Second neighbor					
1 bar	9	7	5	4	3
1000 bar	12	9	6	5	4
5000 bar	17	12	9	7	5

FIG. 9. Geometric autocorrelation functions for $k=2$ (the chord vector) and 400 K at (a) 1 bar and (b) 5000 bar. The ACF simulation data are represented by open symbols with the CONTIN fits denoted by the solid line running through these symbols. The DRTs corresponding to the solid ACF fits are plotted as filled symbols joined by a solid line. A peak in each DRT indicates the time scale of a relaxation process.

sional angle coupling when moving towards higher pressures and lower temperatures (i.e., "restricted" systems). It is emphasized that the second-neighbor torsional angle coupling is consistently counter-rotational with respect to the TT and would have a negative value if plotted in the format of figures such as Figs. 5 and 6. The top two panels of Fig. 7 show the difference in torsional angle coupling between 375 and 475 K as a function of time at 1 and 5000 bar. The lower two panels of Fig. 7 plot the difference in torsional angle coupling between 5000 and 1 bar as a function of time at 375 and 475 K. The square symbols are for the zeroth neighbor and the circles are for second-neighbor torsional angle coupling.

In all panels the initial differences are small, with the maximum difference between systems occurring some time after the triggering transition. The maximum difference between second neighbors is consistently reached before that of the zeroth neighbor for the same system. All differences between the neighbors tend towards zero at long times with the second neighbors converging more rapidly than the zeroth neighbors.

The relaxation time for the zeroth- and second-neighbor torsional angle coupling is plotted in Fig. 8(a), which is defined as the time taken for torsional angle coupling to fall to a background level of ±2. An example of such a decay is illustrated in Fig. 8(b) at 400 K and 1 bar for the zeroth and second neighbors. In Fig. 8(a), the relaxation time data are plotted as a function of temperature at different pressures with filled and open symbols representing zeroth-neighbor and second-neighbor relaxation times, respectively. A trend common to all data is for restrictive systems to remain coupled longer and for the peak magnitude of the coupling to be greater than for less restrictive systems. Comparison with the inverse of the transition rates in Table II reveals that the relaxation time associated with the zeroth-neighbor torsional angle coupling coincides with the average transition time for the system being analyzed. The relaxation times for the

zeroth- and second-neighbors, along with the ratios of second to zeroth neighbors are shown in Tables V and VI. The data show that coupling persists throughout the period between transitions, implying that the chain works continuously to localize the effects of segmental motion. The ratio of second- to zeroth-neighbor torsional angle coupling relaxation times increases with increasing pressure and decreases with increasing temperature.

V. DYNAMICS

A. Geometric autocorrelation functions

The effect of pressure on local polymer dynamics is also addressed by second (P_2) Legendre polynomial autocorrelation functions (ACF)[44] of bond and chord vectors within the chain. The bond, $\mathbf{b}_i$, is calculated as

$$\mathbf{b}_i = \frac{\mathbf{r}_{i+1} - \mathbf{r}_i}{|\mathbf{r}_{i+1} - \mathbf{r}_i|}, \tag{9a}$$

where $\mathbf{r}_i$ denotes the lab frame coordinates of united atom i. The chord, $\mathbf{c}_{i,k}$ vector is constructed from the bond vector as

TABLE VI. Ratio of second- to zeroth-neighbors torsional angle coupling relaxation time for all systems.

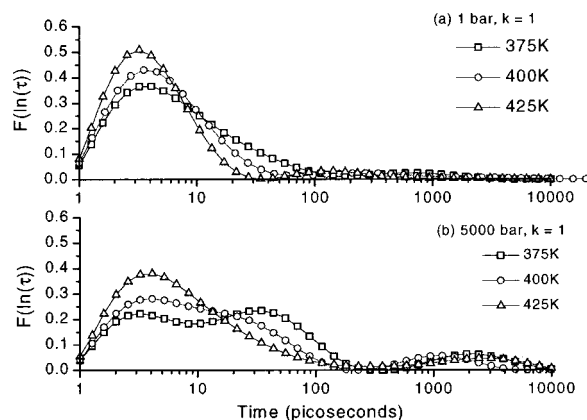|	375 K	400 K	425 K	450 K	475 K
1 bar	0.40	0.41	0.36	0.33	0.30
1000 bar	0.48	0.45	0.40	0.42	0.36
5000 bar	0.50	0.50	0.47	0.47	0.38

FIG. 10. DRTs for $k=1$ (the bond vector) at 375, 400, and 425 K at (a) 1 bar and (b) 5000 bar.
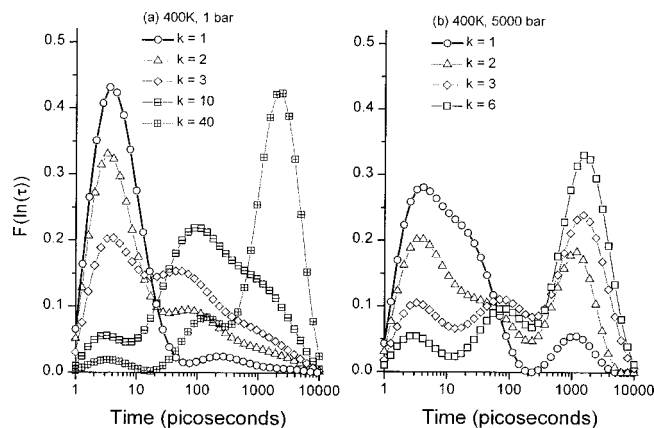
FIG. 11. DRTs at 400 K for (a) 1 bar, $k = 1$ to 40 and (b) 5000 bar, $k=1$ to 6.

$$\mathbf{c}_{i,k} = \frac{\mathbf{b}_i + \mathbf{b}_{i+k}}{|\mathbf{b}_i + \mathbf{b}_{i+k}|}. \tag{9b}$$

k has a range of 1 to N, where N is the number of bonds in the molecule. A chord vector of $c_{i,6}$ would span 6 bonds. Each ACF is analyzed using CONTIN[75,76] which represents their relaxation as a continuous distribution of exponential processes as calculated by Eq. (10)

$$\mathrm{ACF}(t) = \int_{-\infty}^{\infty} F(\ln(\tau)) e^{-t/\tau} d \ln \tau, \tag{10}$$

where $F(\ln(\tau))$ corresponds to a normalized distribution of relaxation times (DRT). Within this model-independent approach, the number and the width of the peaks appearing in the DRTs correspond to the existence of distinct relaxation processes and the dispersion of exponential decays, respectively. A characteristic time for each process appearing in the spectra is associated with the location of its peak in the DRT.

The relaxation of the ACF for the chord vector, at 400 K, is shown as a function of pressure in Fig. 9. The left-hand y axis shows the relaxation of the chord autocorrelation function and the right-hand y axis represents the distribution of relaxation times associated with each pressure. Changes in the curvature of the ACF correspond to peaks in the DRT. The chord vector relaxes at both pressures with primarily two modes of relaxation. The DRTs of the bond ACF vector are shown in Fig. 10 as a function of temperature and pressure. At 1 bar, the DRTs at all temperatures reveal one dominant process at ~4 ps with a narrower width at 425 K. At 5000 bar, it is possible to watch the evolution of an intermediate mode in the relaxation of the bond vector appearing on the 40 ps time scale. As the temperature is reduced, the prominence of the first peak drops and the significance of the intermediate mode increases.

Extending the chord vector incrementally along the length of the backbone affords insight into the effect of coarse graining on segmental dynamics.[77] Analysis has been performed at 1 bar for k values of 1 to 40 (400 K) and at 5000 bar from 1 to 6 (400 K). The data presented within Fig. 11 are representative of the general trends observed. The DRTs show that there is a distinct change in the relaxation of the vector as it encompasses larger sections of the backbone (i.e., k increases). For Fig. 11(a), where $k=1$, one principal mode around 5 ps is observed with a long tail stretching from ~700 ps to several nanoseconds. As k approaches 10, the magnitude of the fast process decreases significantly with a dominant process developing on the time scale of ~100 ps. As k approaches 40, a longer mode evolves on the nanosecond time scale. A significant change in the shape of the DRTs is observed as pressure is increased from 1 to 5000 bar. Figure 11(b) shows three distinct peaks for nearly all values of k: one on the order of picoseconds, one on the order of 100 picoseconds, and a third at times around 2 nanoseconds. Increasing the value of k along the backbone results in a
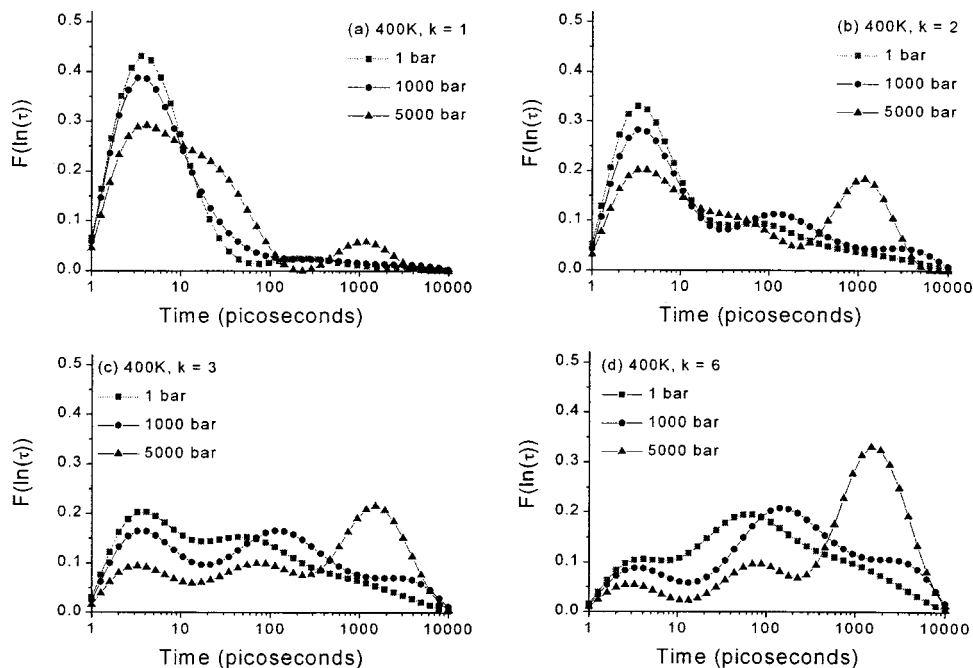

FIG. 12. DRTs at 400 K for pressures of 1, 1000, and 5000 bar. (a) $k=1$, (b) $k=2$, (c) $k=3$, and (d) $k=6$.

change in the magnitude of each mode. As k tends to 6, the fast mode decreases while the intermediate and the slower mode become more pronounced.

Figure 12 shows the effect of pressure on the relaxation of the backbone, as a function of k, at 400 K. For all distances along the backbone it is observed that increasing the pressure results in the development of relaxation processes on longer time scales with a corresponding reduction in the magnitude of the fast process. As seen in Fig. 11(a), the DRT for $k=1$ at 1 bar had a dominant process at 5 ps with a long time tail. However, intermediate and longer modes are clearly seen to develop in Fig. 12(a) when increasing the pressure to 5000 bar. For $k=2$ in Fig. 12(b), all three modes are present for all pressures with the fast mode dominating the DRT except at 5000 bar. For $k=3$ in Fig. 12(c), each pressure reveals a different dominant process. At 1 bar, the fast mode dominates. At 1000 bar, the intermediate mode has the largest amplitude while at 5000 bar the longer mode has the greatest magnitude. For $k=6$ in Fig. 12(c), the intermediate mode dominates the DRT at 1 and 1000 bar, while at 5000 bar the longer mode is most significant. In general, as k increases along with pressure, the intermediate and longer modes play an increasingly significant role in the relaxation of the vector.

VI. CONCLUSIONS

The effect of pressure on the segmental dynamics of melt polyethylene has been addressed. Increasing pressure and decreasing temperature results in decreasing average transition rates and an increasing magnitude of second-neighbor coupled torsional motion. As far as the authors are aware, torsional angle coupling has been examined as a function of a range of Δt values for the first time (i.e., dynamic torsional angle coupling). This analysis quantitatively demonstrates the dynamic nature of torsional angle coupling to a conformational event with zeroth- and second-neighbor coupling observed to persist longer for cooler systems at higher pressures.

The effect of pressure has also been investigated in terms of the reorientation dynamics of the model polyethylene chain on the length scale of a bond vector to a more coarse-grained scale covering larger portions of the chain backbone. As expected, the mechanisms leading to the relaxation of these vectors are a collection of processes including fast motions on the time scale of a few picoseconds and slower motions on the time scale of several nanoseconds. At low temperatures and high pressures a third mechanism is observed for these unentangled chains on a time scale between the fast and slow processes. This mechanism is readily apparent with increased levels of coarse graining [i.e., increasing the k values within Eq. 9(b)], which is similar to that found by Karatasos et al.[44,77] for density-induced modification of local segmental dynamics. The appearance of this intermediate time scale complements the work of Qiu and Ediger[78] using ^{13}C NMR to study the local and global dynamics of unentangled polyethylene melts at ambient pressure. Fits to T_1 and NOE data at ambient pressure required 6–10 Rouse modes, implying the importance of motions with a time scale between the fast segmental motions and the

significantly slower global dynamics to describe satisfactorily the reorientational motion of the C–H bond vectors in their system. Current efforts are correlating the observed pressure effects of the *intramolecular* dynamics with pressure-induced changes in *intermolecular* dynamics through a time-resolved radial distribution function. Future efforts will focus on longer entangled chains in addition to a similar pressure study using a series of backbones that undergoes a systematic change in intramolecular connectivity. These topics will be the source of a future publication.

[1] J. D. Ferry, *Viscoelastic Properties of Polymers*, 3rd ed. (Wiley, New York, 1980).
[2] K. Adachi, Macromolecules **23**, 1816 (1990).
[3] K. Adachi, Y. Imanishi, T. Shinkado, and T. Kotaka, Macromolecules **22**, 2391 (1989).
[4] R. Dejean de la Batie, F. Lauprêtre, and L. Monnerie, Macromolecules **22**, 122 (1989).
[5] S. Glowinkowski, D. J. Gisser, and M. D. Ediger, Macromolecules **23**, 3520 (1990).
[6] F. Lauprêtre, L. Bokobza, and L. Monnerie, Polymer **34**, 468 (1993).
[7] P. Hyde, D. Waldow, M. D. Ediger, T. Kitano, and K. Ito, Macromolecules **19**, 2533 (1986).
[8] P. Hyde, M. D. Ediger, T. Kitano, and K. Ito, Macromolecules **19**, 2253 (1986).
[9] V. Vessier, J.-L. Viovy, and L. Monnerie, Polymer **30**, 1262 (1989).
[10] D. Waldow, B. S. Johnson, P. H. Hyde, M. D. Ediger, T. Kitano, and K. Ito, Macromolecules **22**, 1345 (1989).
[11] D. Waldow, B. S. Johnson, C. L. Babiarz, M. D. Ediger, T. Kitano, and K. Ito, Polym. Commun. **29**, 296 (1988).
[12] S. Adams and D. B. Adolf, Macromolecules **31**, 5794 (1998).
[13] S. Adams and D. B. Adolf, Macromolecules **32**, 3136 (1999).
[14] D. B. Adolf, M. D. Ediger, T. Kitano, and K. Ito, Macromolecules **25**, 867 (1992).
[15] L. Monnerie, Gazz. Chim. Ital. **117**, 139 (1987).
[16] J.-L. Viovy, L. Monnerie, and F. Merola, Macromolecules **18**, 330 (1985).
[17] R. Dejean de la Batie, F. Lauprêtre, and L. Monnerie, Macromolecules **21**, 2045 (1988).
[18] R. Dejean de la Batie, F. Lauprêtre, and L. Monnerie, Macromolecules **21**, 2052 (1988).
[19] G. Williams, Trans. Faraday Soc. **60**, 1556 (1964).
[20] T. A. Weber and E. Helfand, J. Phys. Chem. **87**, 2881 (1983).
[21] E. Helfand, J. Chem. Phys. **54**, 4651 (1971).
[22] E. Helfand, Z. R. Wasserman, and T. A. Weber, Macromolecules **13**, 526 (1980).
[23] T. F. Schatzki, J. Polym. Sci. **57**, 496 (1962).
[24] D. B. Adolf and M. Ediger, Macromolecules **24**, 5834 (1991).
[25] N. Moe and M. D. Ediger, Macromolecules **29**, 5484 (1996).
[26] G. D. Smith and D. Y. Yoon, J. Chem. Phys. **100**, 649 (1994).
[27] G. D. Smith, D. Y. Yoon, W. Zhu, and M. D. Ediger, Macromolecules **27**, 5563 (1994).
[28] G. J. Moro, Chem. Phys. Lett. **173**, 503 (1990).
[29] G. J. Moro, J. Chem. Phys. **94**, 8577 (1991).
[30] G. J. Moro, J. Chem. Phys. **97**, 5749 (1992).
[31] G. Williams, Trans. Faraday Soc. **60**, 1548 (1964).
[32] H. Sasabe and S. Saito, J. Polym. Sci. **6**, 1401 (1968).
[33] D. P. Jing, L. Bokobza, P. Sergot, L. Monnerie, P. Collart, and F. C. de Schryver, Polymer **30**, 443 (1989).
[34] B. D. Freeman, L. Bokobza, and L. Monnerie, Polymer **31**, 1045 (1990).
[35] B. D. Freeman, L. Bokobza, P. Sergot, L. Monnerie, and F. C. de Schryver, J. Lumin. **48−49**, 259 (1991).
[36] A. S. Kulik and K. O. Prins, Polymer **34**, 4629 (1993).
[37] A. S. Kulik and K. O. Prins, Polymer **34**, 4635 (1993).
[38] A. S. Kulik and K. O. Prins, Polymer **34**, 4642 (1993).
[39] A. S. Kulik and K. O. Prins, Polymer **35**, 2307 (1994).
[40] G. Floudas, G. Fytas, T. J. Reisinger, and G. Wegner, J. Chem. Phys. **111**, 9129 (1999).
[41] G. Floudas and T. J. Reisinger, J. Chem. Phys. **111**, 5201 (1999).
[42] G. Floudas, C. Gravalides, T. J. Reisinger, and G. Wegner, J. Chem. Phys. **111**, 9847 (1999).
[43] R. Bharadwaj and R. H. Boyd, Macromolecules **33**, 5897 (2000).

[44] K. Karatasos, D. B. Adolf, and S. D. Hotston, J. Chem. Phys. **112**, 8695 (2000).

[45] T. Pakula, S. Geyler, T. Edling, and D. Boese, Rheol. Acta **35**, 631 (1996).

[46] T. Pakula, K. Karatasos, S. H. Anastasiadis, and G. Fytas, Macromolecules **30**, 8463 (1997).

[47] R. A. Orwoll, in *Physical Properties of Polymers, Handbook* (American Institute of Physics, Woodbury, NY, 1994), Chap. 7.

[48] S. Nosé, Mol. Phys. **52**, 255 (1984).

[49] S. Nosé, J. Chem. Phys. **81**, 511 (1984).

[50] An unpublished study into the stability of p and T as a function of the relaxation coefficients has been carried out. A matrix comprising 48 simulations was generated, each run for 25 ps at a temperature of 400 K and pressures of 1 and 5000 bar. The temperature and pressure relaxation coefficients were tested over a range of three orders of magnitude from 0.01 to 2.00 ps. Acceptable values for coefficients produced an error of less than 0.1% for both temperature and pressure fluctuations. The values used in the current work are taken from this study.

[51] T. Forester and W Smith, CCLRC, Daresbury Laboratory, Daresbury, Warrington, WA4 4AD, England. DL_POLY is a parallel molecular dynamics package developed at Daresbury Laboratory and is a property of the council for the Central Laboratory of the Research Councils, 2.10 ed. (1998).

[52] G. D. Smith, D. Y. Yoon, and R. J. Jaffe, Macromolecules **28**, 5897 (1995).

[53] W. Paul, D. Y. Yoon, and G. D. Smith, J. Chem. Phys. **103**, 1702 (1995).

[54] W. L. Jorgensen and J. Tirado-Rives, J. Phys. Chem. **100**, 14508 (1996).

[55] M. G. Martin and J. I. Siepmann, J. Phys. Chem. B **102**, 2569 (1998).

[56] R. H. Boyd, R. H. Gee, J. Han, and Y. Jin, J. Chem. Phys. **101**, 788 (1994).

[57] R. H. Gee and R. H. Boyd, Comput. Theor. Polym. Sci. **8**, 93 (1998).

[58] D. Rigby and R.-J. Roe, J. Chem. Phys. **87**, 7285 (1987).

[59] E. Helfand, Z. R. Wasserman, and T. A. Weber, J. Chem. Phys. **70**, 2016 (1979).

[60] J. Skolnick and E. Helfand, J. Chem. Phys. **72**, 5489 (1980).

[61] E. Helfand, Science **226**, 647 (1984).

[62] J. Skolnick, Macromolecules **14**, 646 (1981).

[63] R. K. Bharadwaj and R. H. Boyd, J. Chem. Phys. **114**, 5061 (2001).

[64] H. Takeuchi and R.-J. Roe, J. Chem. Phys. **94**, 7446 (1991).

[65] O. Olabisi and R. Simha, Macromolecules **8**, 206 (1975).

[66] L. Yang, D. J. Srolovitz, and A. F. Yee, J. Chem. Phys. **110**, 7058 (1999).

[67] H. Takeuchi and R-J. Roe, J. Chem. Phys. **94**, 7458 (1991).

[68] R.-J. Roe, J. Chem. Phys. **100**, 1610 (1994).

[69] I. Zuniga, I. Bahar, R. Didge, and W. L. Mattice, J. Chem. Phys. **95**, 5348 (1991).

[70] C. Baysal, A. R. Atilgan, B. Erman, and I. Bahar, Macromolecules **29**, 2510 (1996).

[71] C. Bennemann, W. Paul, K. Binder, and B. Dunweg, Phys. Rev. E **57**, 843 (1998).

[72] T. Haliloglu, I. Bahar, and B. Erman, Macromolecules **29**, 8942 (1996).

[73] W. Paul, G. D. Smith, and D. Y. Yoon, Macromolecules **30**, 7772 (1997).

[74] G. D. Smith, W. Paul, D. Y. Yoon, A. Zirkel, J. Hendricks, and D. Richter, J. Chem. Phys. **107**, 4751 (1997).

[75] S. Provencher and V. Dovi, J. Biochem. Biophys. Methods **1**, 313 (1979).

[76] S. Provencher, Comput. Phys. Commun. **27**, 213 (1982).

[77] K. Karatasos and D. B. Adolf, J. Chem. Phys. **112**, 8225 (2000).

[78] X. Qiu and M. D. Ediger, Macromolecules **33**, 490 (2000).